Pergamon

Int. J. Mach. Tools Manufact. Vol. 34, No. 8, pp. 1079–1090, 1994

0890–6955/94$7.00 + .00

0890–6955(93)E0016-X

INFRARED SENSING OF FULL PENETRATION STATE IN GAS TUNGSTEN ARC WELDING

H. E. BEARDSLEY,† Y. M. ZHANG† AND R. KOVACEVIC†

(*Received* 8 *February* 1993; *in final form* 1 *December* 1993)

Abstract—The objective of this study is to present an applicable top-side infrared sensing technique for the prospective closed-loop control of weld penetration in gas tungsten arc welding (GTAW). A model is developed to calculate the full penetration state, which is specified by the back-side bead width, from the sensed infrared images. To ensure the model validity in the prospective closed-loop control, the experiments, which generate the data for the model identification, are conducted under the experimental conditions that will be encountered during practical closed-loop control of the welding process. The heat transfer condition and electrode tip angle may vary during welding or from case to case. Also, the control variables which are used to adjust the weld process in order to reach the required weld penetration will also change. In many cases, the current can be employed as an on-line adjustable control variable because of the implementation ease, when the welding speed and arc length are maintained at the preset values. Thus, different currents, workpiece sizes, and electrode tip angles are arranged in the experiments to emulate the possible current adjustments, case to case heat transfer variations, and electrode wear. The infrared characteristics of the effects of these parameters are extracted to regress the full penetration state. Finally, the back-side weld width (the full penetration state) is calculated using the resultant model from the sensed infrared data.

1. INTRODUCTION

MEASURE OF weld penetration plays a crucial role in the closed-loop control of weld quality. A number of concepts have been presented to monitor the weld penetration. These concepts include weld pool oscillation [1–4], ultrasonic sensing [5–7], infrared sensing [8, 9], bead width sensing [10, 11], radiographic sensing [12, 13], back-side bead width sensing [14, 15] and back-side infrared sensing [16]. We note that the first four concepts are based on top-side sensing, which is of interest to us.

Pool oscillation can be used to distinguish the complete penetration case from the incomplete one [2, 3]. However, to extract the accurate pool size, more information may have to be used [4]. In the case of ultrasonic sensing, contact transducers have been used [6, 7] which are inconvenient in practical welding. Among the existing top-side sensing techniques, the infrared approach may be a promising method. Infrared sensing of the welding process has been extensively studied at the Auburn University. The attention was focused on the partial penetration mode in gas metal arc welding (GMAW).

The subject of our study is the full penetration in GTAW, the state of which is described by the back-side weld width b_b (see Fig. 1). It has been found that b_b can

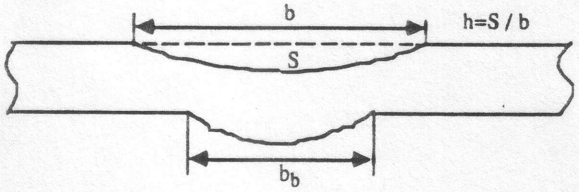

FIG. 1. A traverse cross section of full penetration weld. S is the depression area at the cross section. b is the weld width. $h = S/b$ is the average depth of depression. b_b is the back-side weld width which specifies the state of full penetration. The weld pool surface is not shown in this cross section.

†Center for Robotics and Manufacturing Systems and Department of Mechanical Engineering, University of Kentucky, Lexington, KY 40506, U.S.A.

be sufficiently described by a top-side geometric parameter $h=S/b$, namely the average top-side weld depression depth, through a simple linear relationship [17]. Therefore, we presented a top-side 3D vision-based full penetration sensing technique to monitor the full penetration (see Fig. 2) [18, 19]. The weld depression corresponding to the laser stripe is measured to provide an accurate feedback of the full penetration control system [20]. However, if the welding temperature field is sensed, more information will be obtained earlier. A significant improvement in the performance of the control system will be expected in terms of the response speed. Consequently, a high performance hybrid closed-loop control system can be expected.

In order to establish a valid model, an analysis is performed in this paper to determine the proper experimental conditions under which the model will be applied. It is found that the current, heat transfer condition and electrode tip angle may frequently change from case to case or during welding. Thus, the experiments are conducted accordingly. The established model based on the respective experiments is expected to be applied in a prospective closed-loop control system.

2. INFRARED SENSING OF WELDING PROCESSES

Infrared sensing has been used to measure the cooling rate of the weld pool. Lukens and Morris [21] utilized commercial infrared sensing equipment to monitor the weld metal cooling rate. In the work by Doong *et al.* [22] the surface temperatures near the end part of the molten pool were measured by two infrared temperature sensing devices to calculate the cooling rate.

Several important studies concerning infrared sensing of welding processes have been performed by Chin *et al.* [8, 9, 23]. Two different approaches were developed to monitor the bead width, but both relied on identification of the solid–liquid metal interface. In the first approach [23] a linescan mode was used to detect the solid–liquid interface in the thermal profile of the plate being welded. The interface was easily recognized because a definite change in slope of the temperature profile existed at the interface due to the differing emissivities of the solid and liquid metal. Bead width measurement in the second approach [23] was accomplished by plotting the absolute temperature distribution of the weld zone. Knowing the melting point of the workpiece material, a threshold temperature was selected above which the metal was in its molten state.

Infrared sensors have also showed potential for detecting variation in weld penetration [8, 9, 23]. To our knowledge, the top-side infrared sensing of weld pen-

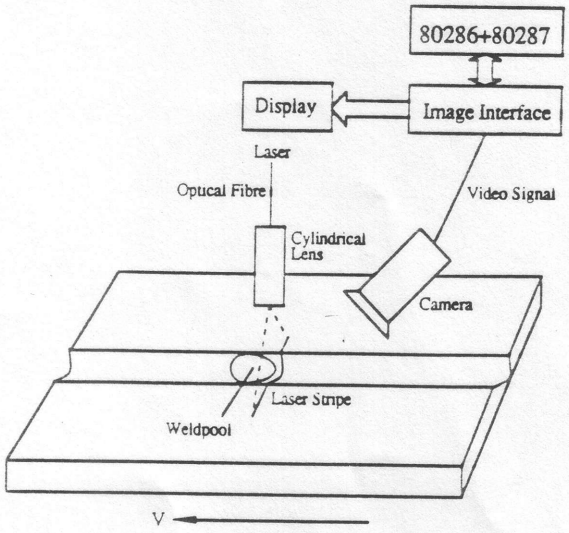

FIG. 2. Three-dimensional vision sensing of full penetration. The intersection of the laser and weld path can be sensed to compute S, b, and h shown in Fig. 1.

etration has been explicitly explored only in these papers. Despite the valuable contributions, unvaried experimental conditions were used. To ensure the validity of a resultant model for prospective closed-loop control, the use of varied conditions seems more appropriate. In a more recent work [23], varied plate thicknesses were employed. However, no mathematical models have been extracted based on these experiments to calculate the weld penetration from the infrared images. Thus, the model establishment is addressed in this study because of its fundamental role in developing an infrared based closed-loop system for weld penetration control.

3. EXPERIMENTAL SET-UP AND PROCEDURE

The experiments for this investigation were conducted on mild steel plates using tungsten inert gas welding. The schematic of the experimental set-up is illustrated in Fig. 3. The welding equipment consisted of a constant-current rectified a.c. power supply (Lincoln's Idealarc TIG welder-model 300/300), with a range of 40–300 A, and a water-cooled GTAW torch operating in a d.c. electrode negative mode. The electrode diameter was 3 mm. High purity argon was employed as the shielding gas at a flow rate of 10 l/min. Constant welding speed (2 mm/sec) and arc length (2.5 mm) were utilized to conduct all the experiments in this investigation.

The infrared camera employed to measure the surface temperature distributions was Inframetric's infrared scanning camera-model 600. The camera incorporates electromechanical servos to perform horizontal and vertical scanning which produces a high scan rate (8 kHz horizontal and 60 Hz vertical). Thermal radiation enters the evacuated scan module through a germanium window where it is deflected by the horizontal and vertical scan galvanometers. It exits through a second window and passes through the focus lens on to the detector. The mercury/cadmium/telluride infrared detector is cooled to 77 K with liquid nitrogen.

Invisible infrared radiation emitted from the top surface of the workpiece is converted into equivalent voltage signals which represent the temperature field. These signals are amplified and transferred to a monitor and a video cassette recorder. During data processing, the video signals are digitized by a frame grabber into 8-bit 256×240 digital matrices. An image processing algorithm has been developed to map temperatures to the specified gray scales and locate the required isotherms. The infrared parameters required to calculate the weld penetration are then extracted from the isotherms. The image acquisition, which may take from 33.3 msec up to about 66.6 msec at the standard frame rate of the video system and image processing can be completed in 90 msec on the PC486DX66-based computer and image system. For GTAW addressed in this paper, this rate is adequate [24].

An important mission of the image processing is to locate the isotherm corresponding to the weld pool. If the emissivities of the weld pool and solid material are exactly known, this isotherm will be easily found based on the melting point of the material. However, the available emissivity data of the weld pool is insufficient and imprecise. Also, the emissivity of the solid material is severely influenced by the color of the

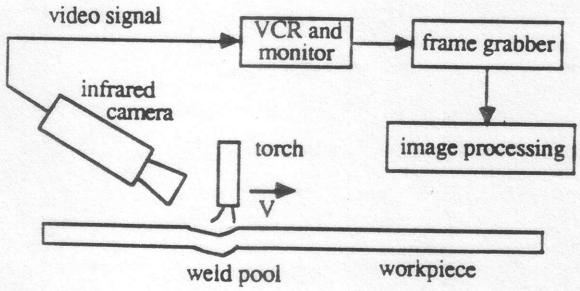

FIG. 3. Experimental set-up for infrared sensing of GTA welding. In order to illustrate the possible depression associated with the GTA weld pool, the workpiece is shown by a cross section. The weld pool surface is, therefore, not shown in the figure.

material which changes with the oxidation. Thus, another method must be used to determine the weld pool.

It has been shown by Kraus [25] that the emissivity of a GTAW weld pool varies in a very small range and can be regarded as a constant. Also, it can be shown through numerical calculation [25] that the calculated temperature nearly linearly varies with the assumed emissivity. Furthermore, the weld pool boundary can be clearly sensed and extracted using a novel technology developed in our previous study [24]. Thus, the pool emissivity can be fitted by comparing the resultant infrared isotherm and extracted pool boundary. (This principle is shown in Fig. 4). Consequently, the isotherm corresponding to the pool boundary can be located from the sensed images.

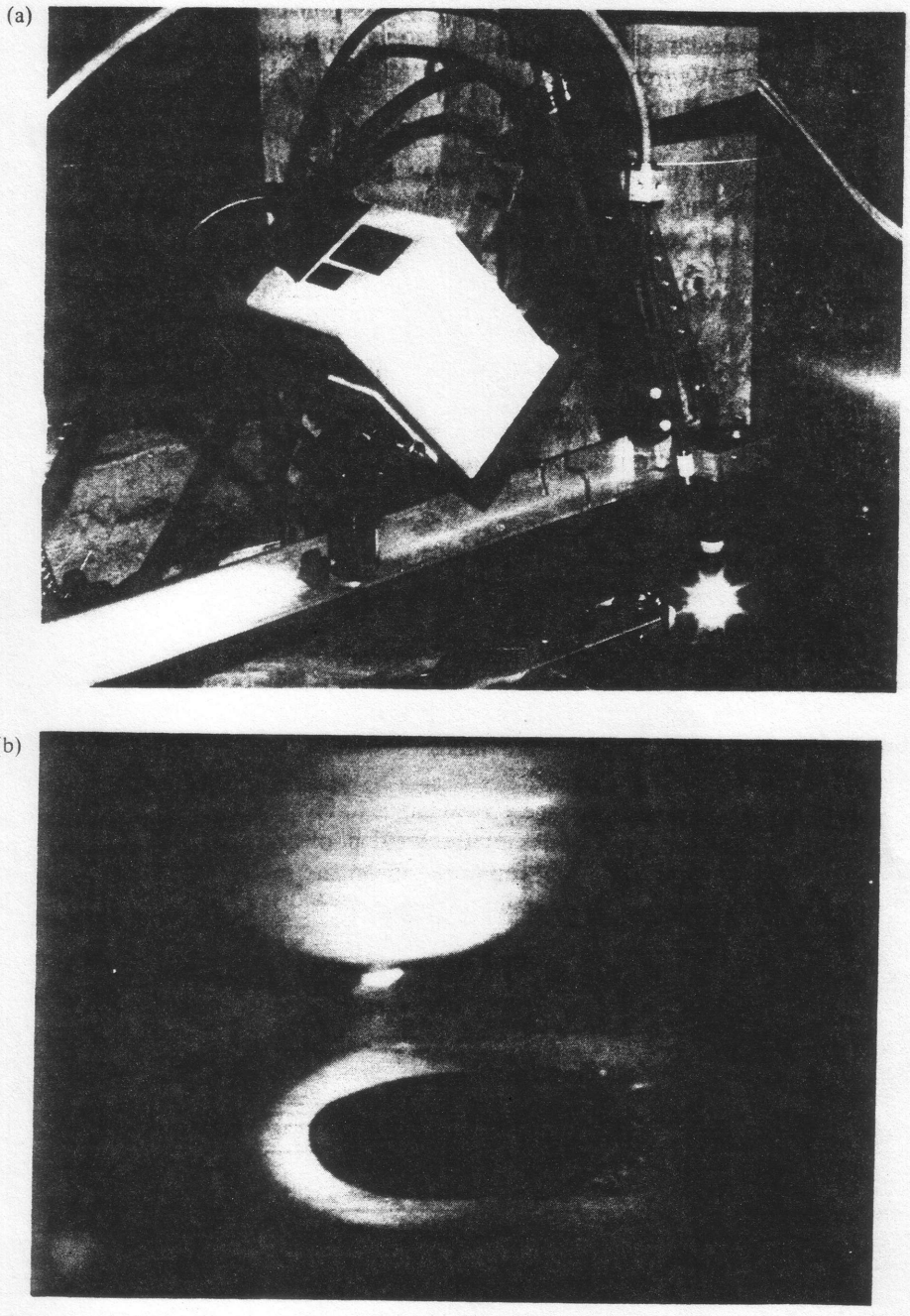

FIG. 4. Calibration principle of emissivity for weld pool boundary determination. (a) Sensing system. (b) weld pool boundary.

(c)

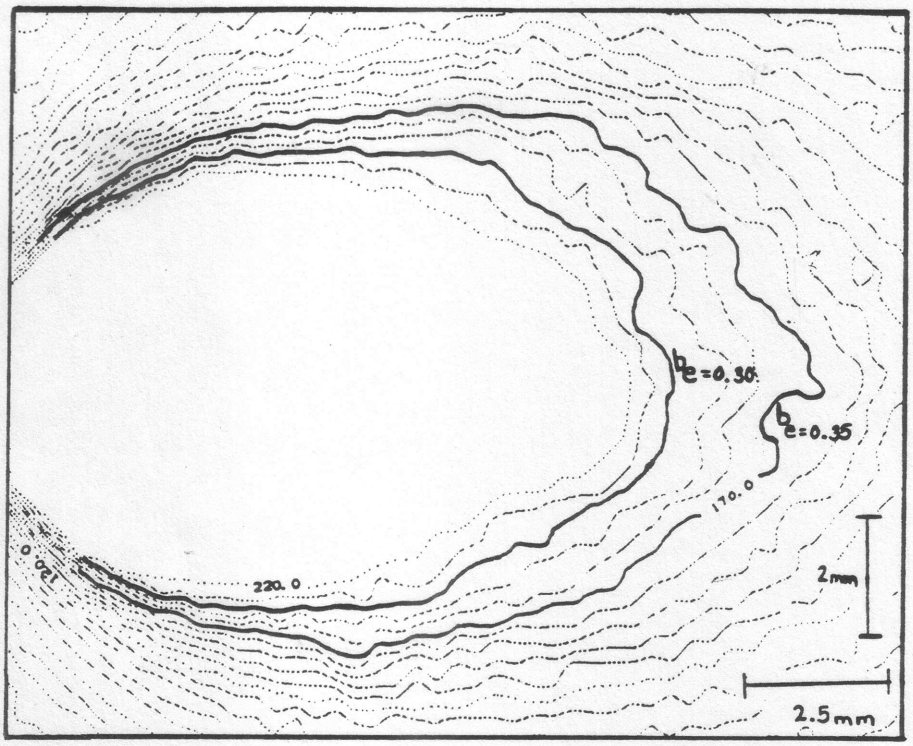

FIG. 4. Continued.

e: emissivity of the weld pool. *b*: boundary of the weld pool.

(c) Isotherms. The temperatures of isotherms can be determined if the emissivity is known. For any assumed emissivity of weld pool, which is regarded as a constant [23], the pool boundary can be located. The emissivity of the weld pool is selected by generating an optimal approximation to the accurate measurement.

The objective of the experiments in this study is to reveal the infrared characteristics of variations in various welding parameters of interest. The parameters which influence the full penetration state may include the welding current, arc length, welding speed, heat transfer condition, electrode tip angle (or convex), butt gap, flow rate of shielding gas, plate thickness, surface condition, etc. For a specific welding operation, the arc length, welding speed, flow rate of shielding gas, and plate thickness can be well controlled or assumed to be certain. We can also assume that the surface has been well prepared. However, the heat transfer condition, electrode tip angle, and butt gap may change from case to case or even during welding owing to possible asymmetry of the weld path on the workpiece, ambient temperature variation, electrode wear and joint-preparation imperfection. Also, the welding current will be used as the control variable and, therefore, will vary during closed-loop control. Thus, different currents, heat transfer conditions, electrode tip angles, and butt gaps may be encountered during a closed-loop control process. They must be emulated in the experiments which are conducted to acquire the data for developing the relationship between the infrared characteristics and the back-side bead width. In this study, for the sake of simplicity, the variation in butt gap will not be included. Comparative welding conditions were arranged. For each parameter, a reference level was given. The reference workpiece size, electrode tip angle, and current were selected to be (200 mm × 100 mm × 3 mm), 60°, and 120 A, respectively. The reference current was determined by preliminary experiments to ensure proper states of full penetration when the welding parameters vary in the given ranges. To emulate the possible variation in heat transfer condition, different sizes of workpieces were used (see Table 1). The resultant experimental parameters are listed in Table 1. It can be seen that different currents, heat transfer

TABLE 1. EXPERIMENTAL PARAMETERS

Experiment	Parameters
105 A	105-A, 60°, 20 cm × 10 cm × 0.3 cm
Reference	120 A, 60°, 20 cm × 10 cm × 0.3 cm
Poor heat trans.	120 A, 60°, 20 cm × 7 cm × 0.3 cm
Poorest heat trans.	120 A, 60°, 20 cm × 6 cm × 0.3 cm
30° tip angle	120 A, 30°, 20 cm × 10 cm × 0.3 cm
80° tip angle	120 A, 80°, 20 cm × 10 cm × 0.3 cm
132 A	132 A, 60°, 20 cm × 10 cm × 0.3 cm

Welding speed: 2 mm/sec. Rate of argon flow: 10l/min. Arc length: 2.5 mm.

conditions (workpieces of different sizes), and electrode tip angles have been incorporated.

4. INFRARED CHARACTERISTICS OF EFFECTS OF WELDING PARAMETERS

In this section, we will find the infrared characteristics associated with the changes in welding parameters. It would be ideal to find an independent infrared characteristic for each welding parameter of interest for the sake of decoupling the effects of welding parameters. However, this will be difficult since virtual couplings may exist between different welding parameters in determining the welding thermal distribution. Thus, a certain infrared characteristic may be used to describe the influence of multi-parameters on the thermal distribution.

In each experiment, the welding duration was about 70 sec. The sampling period is selected to be 3 sec. Twenty images were sampled from each workpiece. The first reading was recorded 5 sec after the welding began.

It is well known that the most important weld parameter which determines the weld thermal field is the welding current in the case of a constant welding speed. An increment of welding current will generate an increase in the power input and result in a larger weld pool area [26]. Thus, the weld pool area can probably be selected as an infrared characteristic to represent the effect of the welding current. In order to confirm this assumption, the weld pool areas were calculated.

In Fig. 5, the weld pool areas associated with the current variation experiments are depicted. It can be seen that although the weld pool areas slightly vary with time,

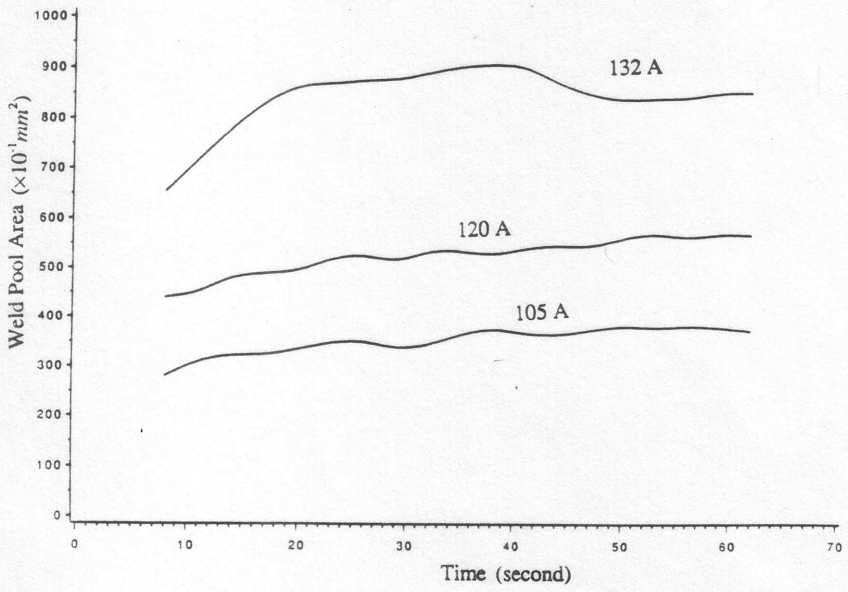

FIG. 5. Weld pool area under different weld currents.

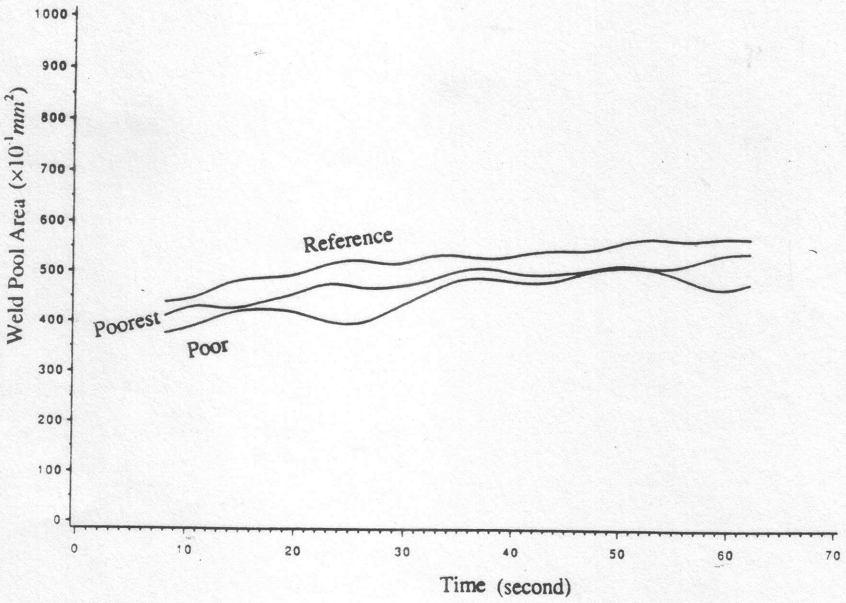

FIG. 6. Weld pool area under different heat transfer conditions.

there is a clear difference in the weld pool areas associated with different welding currents.

In Fig. 6, the weld pool areas are plotted for the experiments under different heat transfer conditions. In this case, the difference in weld pool areas with respect to different heat transfer conditions are small, compared with the difference in Fig. 5. It is known that the heat transfer condition is also an important parameter which influences the welding process. However, since the weld pool is formed very rapidly, it appears that the weld pool will primarily be determined by the heat input. Thus, the influence of the heat transfer condition on the weld pool area will not be significant. In fact, it has been found that the top-side weld width is not sensitive to the variation of heat transfer condition in stainless steel GTAW [19]. When the electrode tip angle changes, a small change in the weld pool area is observed (see Fig. 7). This suggests that the

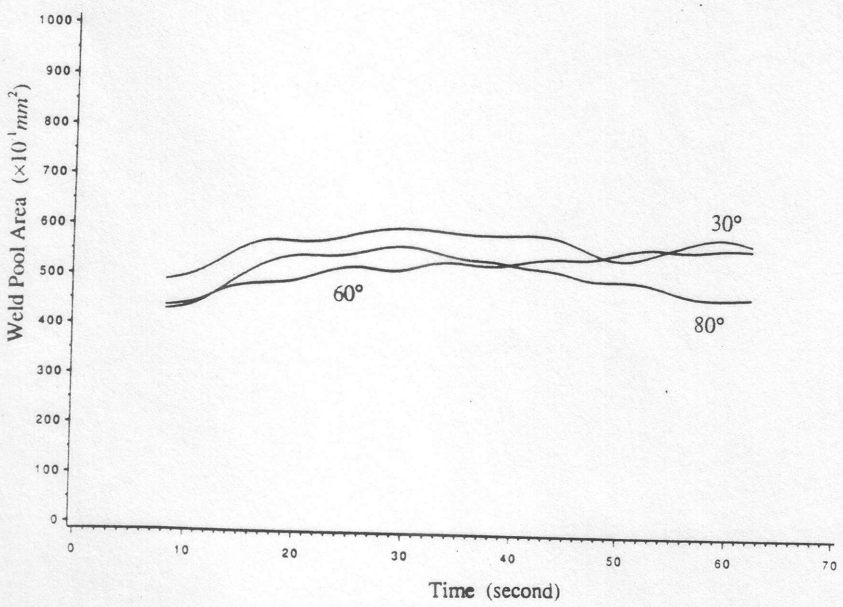

FIG. 7. Weld pool area under different electrode tip angles.

weld pool area can be selected as an infrared characteristic. This characteristic is mainly determined by the welding current, but also influenced by the electrode tip angle.

Although the heat transfer condition does not significantly influence the weld pool area or the top-side weld width, it is an important parameter in determining the full penetration state [19, 20, 24]. The heat transfer condition affects the full penetration state when the heat from the arc energy transfers through the workpiece. It is apparent that the area in a certain temperature range $[T_1, T_2]$, where T_1 and T_2 are two temperatures lower than the melting temperature and $T_1 < T_2$, increases as the heat transfer condition becomes poor. Theoretically, T_1 and T_2 can be any values that meet the above requirement. However, in order to obtain robust measurements, $T_2 - T_1$ should not be too small and both T_1 and T_2 must be within the acceptable range of measurement of the infrared camera. For example, T_1 may be selected to represent the heat affected zone. However, the temperature with respect to the heat affected zone may vary with the material. In the present paper, T_1 and T_2 are selected as 600°C and 1300°C, and the corresponding area is called the surrounding area. (The proper selection of T_1 and T_2 will be different when the constant welding parameters, for example, welding speed, material thickness, and type of material etc., change because of the significant influences these parameters have on the resultant weld thermal field [26]. The selection should be made based on the resultant modeling validity in explaining the data.) It appears that this surrounding area is a promising candidate for the infrared characteristic of heat transfer condition. However, further investigation shows that the surrounding area should also be related to the weld pool area. The larger the weld pool area is, the larger the surrounding area is, under a given heat transfer condition. Thus, a surrounding area to weld pool area ratio is proposed as another alternative:

$$\lambda = S_s/S_p \tag{1}$$

where S_p and S_s are the weld pool area and the surrounding area, respectively. This ratio is called the area ratio. It must be pointed out that, although λ is defined using the weld pool area S_p, λ may not be significantly influenced by S_p. This is due to the fact that S_s is also influenced by S_p. We expect that S_s/S_p will not be affected by S_s and will primarily be determined by the heat transfer condition.

In Fig. 8, the area ratios associated with different heat transfer conditions are plotted. It can be seen that although the differences between the workpiece widths are small, the area ratios are well separated. Also, the ratios are almost flat along the seams while S_p varies. Thus, the area ratio is not significantly influenced by S_p and is mainly determined by the heat transfer condition.

Figure 9 depicts the area ratios for the current variation experiments. It can be seen that the welding currents do not significantly influence the ratio. However, this ratio is affected by the electrode tip angle (see Fig. 10).

The influence of the electrode tip angle on welding processes is not well known. Basically, the tip angle, or the electrode shape, affects the arc distribution and the maximum arc pressure [26]. However, a variety of results have been obtained from

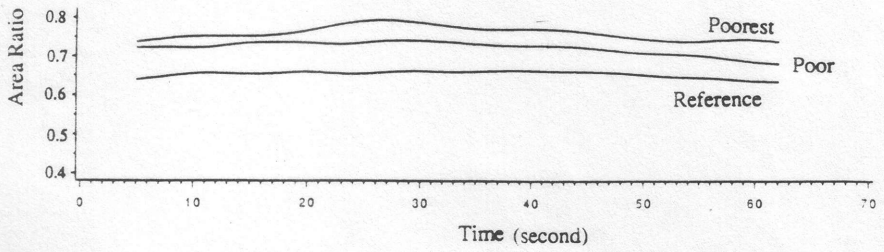

FIG. 8. Modified area ratios under different heat transfer conditions.

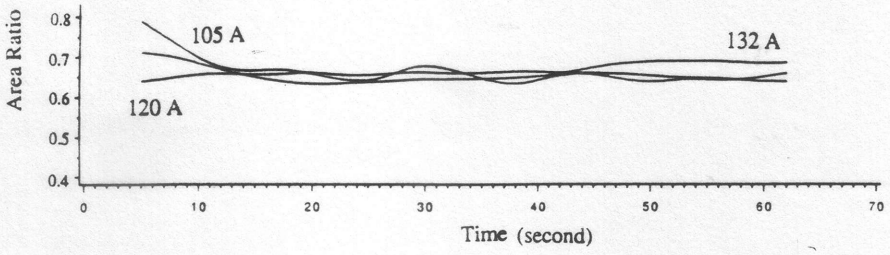

FIG. 9. Modified area ratios under different welding currents.

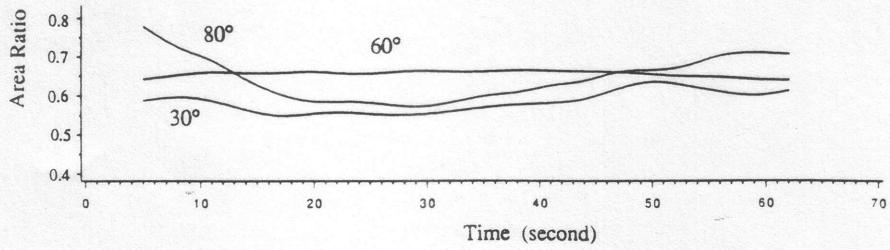

FIG. 10. Modified area ratios under different electrode tip angles.

various studies of the effects of electrode tip angle on GTA weld shape [26]. In our three experiments concerning the electrode tip angle, the back-side weld width associated with the 30° tip angle is the largest.

If the area ratio is selected as an infrared characteristic, it will primarily pair with the heat transfer condition and will be influenced by the tip angle. Figure 11 shows plots of the back-side weld widths associated with the experiments performed with different electrode tip angles. As a matter of fact, although a smaller area ratio is associated with the case of the 30° tip angle, its weld pool area is significantly larger. As for the difference between the back-side weld widths with respect to the 60° and 80° tip angles, this can be explained by the larger area ratio with respect to the 60° tip angle and the similar weld pool areas. Thus, we can principally employ the weld pool area and the area ratio to describe the effect of the electrode tip angle on the thermal distribution.

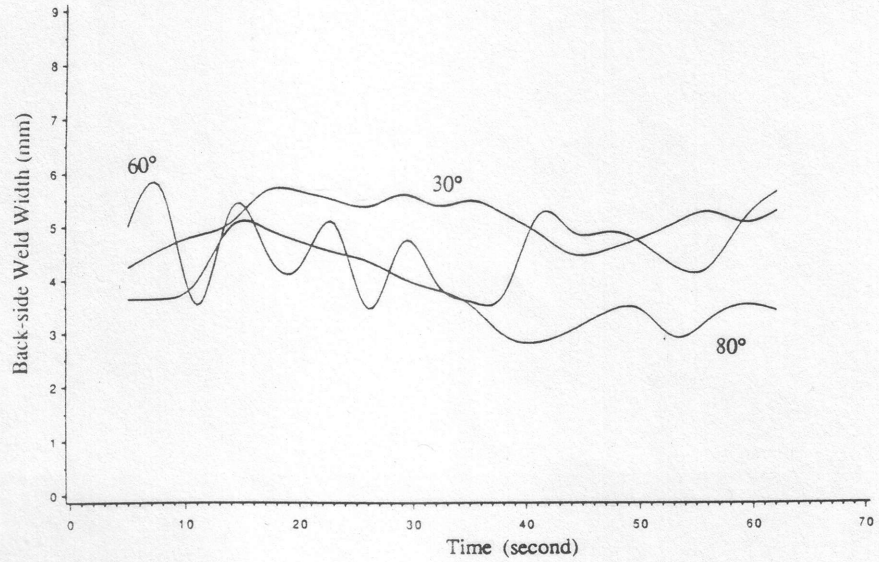

FIG. 11. Back-side bead widths under different electrode tip angles.

Based on the discussion in this section, it can be concluded that the weld pool area and the area ratio can be selected as infrared characteristics of the effects of the welding parameters of interest. The weld pool area is primarily paired with the welding current and the area ratio with the heat transfer condition. The effect of the tip angle may be decomposed into two components, one corresponding to an equivalent welding current and another to an equivalent heat transfer condition.

It must be pointed out that the infrared characteristic description of the effects of welding parameters is primarily utilized to enable the development of a mathematical model of the relationship between the surface thermal distribution and the full penetration state. If an adequate description can be obtained for the effects of welding parameters of interest, the validity of these characteristics will be assured.

5. MATHEMATICAL MODELING

In order to measure the full penetration state, a mathematical model needs to be obtained to calculate the back-side weld width based on the infrared characteristics. A statistical analysis will be performed in this section to acquire such a model based on the measured back-side weld width and the corresponding weld pool areas and area ratios (see Figs 5–10). Although seven experiments have been conducted to extract the infrared characteristics, full penetration throughout the weld was present in only five of the workpieces. The measurements associated with the fully penetrated workpieces depicted in Fig. 12 are utilized. For the sake of simplicity, the discrete time is used throughout this section.

Consider the following linear model:

$$b_b(k) = \alpha_0 + \sum_{j=1}^{n} \alpha_j x_j(k) + \varepsilon(k), \tag{2}$$

where k ($k = 1, 2, \ldots, N$) is the discrete time, x_j ($j = 1, \ldots, n$) are the regressive factors which consist of the possible function of S_s and λ, $N = 100$ is the sample size and $\{\varepsilon(k)\}$ is a white noise sequence. The least squares method is utilized to estimate the parameters α_j in equation (2). The model structure is determined (i.e., the regressive factors are chosen) by the F-test.

Let

$$x(k) = (1, x_1(k), \ldots, x_n(k))^T \tag{3}$$

$$\alpha(k) = (\alpha_0, \alpha_1(k), \ldots, \alpha_n(k))^T \tag{4}$$

$$\Phi = (x(1), \ldots, x(N))^T \tag{5}$$

$$B_b = (b_b(1), \ldots, b_b(N))^T. \tag{6}$$

The least squares estimate of α is:

$$\hat{\alpha}_{LS} = (\Phi^T\Phi)^{-1}\Phi^T B_b. \tag{7}$$

By statistical analysis, the following model is obtained:

$$b_b = -0.0995 + 0.007177 S_p + 1.4448\lambda^{2.3}. \tag{8}$$

The variance of the error is 0.3682 mm^2. The model-calculated and measured values of b_b are depicted in Fig. 12 for comparison. It can be seen that although the welding parameters vary in a wide range, the back-side weld width b_b has been sufficiently described by the model (equation (8)) using the infrared characteristics in most cases. However, it is known that the thermal inertia is great during welding. Thus, when the

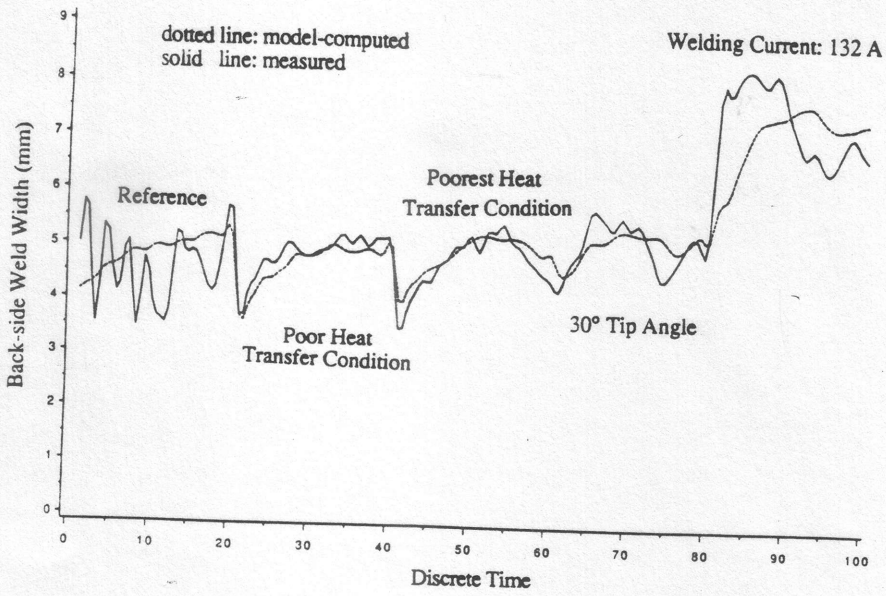

FIG. 12. Measured and model-computed back-side bead widths.

weld penetration changes rapidly, the infrared data often cannot generate a sufficient prediction. This can be seen from the experiments associated with the reference condition and 132 A current in Fig. 12. But, in most applications, the welding conditions may not vary so rapidly. In these cases, the infrared sensing is promising.

6. CONCLUSIONS

Variations of welding parameters that are frequently encountered in practical welding have been considered in the experiments to raise the validity of the resultant model in prospective infrared based closed-loop control systems for complete penetration. The weld pool area and the area ratio have been extracted as the infrared characteristics to describe the effect of welding parameters of interest. It has been shown that the resultant empirical model can describe the back-side weld width (a measurement of the full penetration state) using the characteristics generated from the infrared images. When the process variations are not too abrupt, the accuracy is satisfactory. Since this model is established based on the practical welding conditions, it is expected that this model can be applied in a prospective top-side infrared closed-loop control system for complete penetration.

Acknowledgement—The authors would like to thank Dr C. J. Cremers, Dr K. Saito and Mr Y. S. Chen for their collaboration in conducting this study. The financial support of the Center for Robotics and Manufacturing Systems is greatly appreciated.

REFERENCES

[1] R. J. RENWICK and R. W. RICHARDSON, Experimental investigation of GTA weld pool oscillations, *Welding J.* **62**, 29s–35s (1983).
[2] Y. H. XIAN and G. DEN OUDEN, Weld pool oscillation during GTA welding of mild steel, *Welding J.* **72**, 428s–434s (1993).
[3] Y. H. XIAN and G. DEN OUDEN, A study of GTA weld pool oscillation, *Welding J.* **69**, 289s–293s (1990).
[4] A. S. TAM and D. E.HARDT, Weld pool impedance for pool geometry measurement: stationary and nonstationary pools, ASME *J. dyn. Syst. Meas. Control* **111**, 545–553 (1989).
[5] D. E. HARDT and J. M. KATZ, Ultrasonic measurement of weld penetration, *Welding J.* **63**, 273s–281s (1989).
[6] R. FENN, Ultrasonic monitor and control during arc welding, *Welding J.* **64** (9), 18–22 (1985).
[7] N. M. CARLSON and J. A. JOHNSON, Ultrasonic sensing of weld pool penetration, *Welding J.* **67**, 239s–246s (1988).
[8] S. NAGARAJAN, W. H. CHEN and B. A. CHIN, Infrared sensing for adaptive arc control, *Welding J.* **68**, 462s–466s (1989).
[9] W. CHEN and B. A. CHIN, Monitoring joint penetration using infrared sensing techniques, *Welding J* **69**, 181s–185s (1990).

[10] W. F. CLOCKSIN, *et al.*, *Int. J. Robotics Res.* **4**, 13–26 (1985).
[11] A. P. KENNETH and M. P. SCOTT, Coaxial vision-based weld pool width control, *PED* Vol. 51, *Welding and Joining Processes*, pp. 251–264. ASME (1991).
[12] S. I. ROKHLIN and A. C. GUU, Closed-loop process control of weld penetration using real-time radiography, *Mater. Evaluation*, 363–369 (March 1989).
[13] S. I. ROKHLIN and A. C. GUU, Computerized radiographic sensing and control of an arc welding process, *Welding J.* **69**, 83s–97s (1990).
[14] D. GARLOW, Closed loop control of full penetration welds using optical sensing of back bead width, S. M. Thesis, Dept. of M. E., MIT (1982).
[15] A. SUZUKI, D. E. HARDT, and L. VALAVANI. Application of adaptive control theory to on-line GTA weld geometry regulation, *ASME J. dyn. Syst. Meas. Control* **113**, 93–103 (1991).
[16] J. B. SONG and D. E.HARDT, Multivariable adaptive control of bead geometry in GMA welding, *PED*-Vol. 51, *Welding and Joining Processes*, pp. 123–134, ASME (1991).
[17] Y. M. ZHANG *et al.*, Determining joint penetration in GTAW with vision sensing of weld face geometry, *Welding J.* **72**, 463s–469s (1993).
[18] Y. M. ZHANG, R. KOVACEVIC, L. WU and D. H. CHEN, Controlling welding penetration in GTAW using vision sensing and adaptive control technique, *Trans. NAMRI/SME*, **20**, 317–323 (1992).
[19] Y. M. ZHANG, R. KOVACEVIC and L. WU, Sensitivity of front-face weld geometry in representing the full penetration, *Proc. Instn. Mech. Engrs, Part B: J. Engng Manufact.*, **206**, 191–197 (1992).
[20] Y. M. ZHANG, R.KOVACEVIC and L. WU, Closed-loop control of weld penetration using front-face vision sensing, *Proc. Instn Mech. Engrs, Part I: J. Syst. Engng Control* **207**, 27–34 (1993).
[21] W. E. LUKENS and R. A. MORRIS, Infrared temperature sensing of cooling rates for arc welding control, *Welding J.* **61**, 27–33 (1982).
[22] J. L. DOONG, C. S. WU and J. R. HWANG, Infrared temperature sensing of laser welding, *Int. J. Mach. Tools Manufact*, **31**, 607–616 (1991).
[23] S. NAGARAJAN, P. BANERJEE, W. H. CHEN and B. A. CHIN, Control of the welding process using infrared sensors, *IEEE Trans. Robotics Automation* **8**, 86–93 (1992).
[24] R. KOVACEVIC, Y. M. ZHANG and S. RUAN, Sensing and control of weld pool geometry for automated welding, (accepted for publication), ASME *J. Engng Ind.*
[25] H. G. KRAUS, Optical spectral radiometric/laser reflection method for noninvasive measurement of weld pool surface temperatures, *Opt. Engng* **26**, 1183–1190 (1987).
[26] P. BURGARDT and C. R. HEIPLE, Interaction between impurities and welding variables in determining GTA weld shape, *Welding J.* **65**, 150s–155s (1986).